Engineering Fracture Mechanics 77 (2010) 170–181

Contents lists available at ScienceDirect

Engineering Fracture Mechanics

journal homepage: www.elsevier.com/locate/engfracmech

J–T characterized stress fields of surface-cracked metallic liners bonded to a structural backing – I. Uniaxial tension

Shawn A. English [a], Nagaraj K. Arakere [a,*], Phillip A. Allen [b]

[a] *Department of Mechanical and Aerospace Engineering, University of Florida, Gainesville, FL, USA*
[b] *NASA Marshall Space Flight Center, MSFC, Huntsville, AL, USA*

ARTICLE INFO

Article history:
Received 7 June 2009
Received in revised form 18 September 2009
Accepted 28 September 2009
Available online 4 October 2009

Keywords:
Constraint effects
Finite element analysis
Ductile fracture
J-integral
Pressurized components

ABSTRACT

Surface crack-tip stress fields in a tensile loaded metallic liner bonded to a structural backing are developed using a two-parameter *J–T* characterization and elastic–plastic modified boundary layer (MBL) finite element solutions. The Ramberg–Osgood power law hardening material model with deformation plasticity theory is implemented for the metallic liner. In addition to an elastic plate backed surface crack liner model, elastic–plastic homogeneous surface crack models of various thicknesses were tested. The constraint effects that arise from the elastic backing on the thin metallic liner and the extent to which *J–T* two parameter solutions characterize the crack-tip fields are explored in detail. The increased elastic constraint imposed by the backing on the liner results in an enhanced range of validity of *J–T* characterization. The higher accuracy of MBL solutions in predicting the surface crack-tip fields in the bonded model is partially attributed to an increase in crack-tip triaxiality and a consequent increase in the effective liner thickness from a fracture standpoint. After isolating the effects of thickness, the constraint imposed by the continued elastic linearity of the backing significantly enhanced stress field characterization. In fact, *J* and *T* along with MBL solutions predicted stresses with remarkable accuracy for loads beyond full yielding. The effects of backing stiffness variation were also investigated and results indicate that the backing to liner modulus ratio does not significantly influence the crack tip constraint. Indeed, the most significant effect of the backing is its ability to impose an elastic constraint on the liner. Results from this study will facilitate the implementation of geometric limits in testing standards for surface cracked tension specimens bonded to a structural backing.

1. Introduction

Surface cracks are among the most common flaws present in structural components and frequently the most critical in terms of limiting structural life, for both ductile and brittle materials [1,2]. Fracture prediction for through-thickness cracks has been studied extensively using both single parameter (*K* for brittle fracture and *J* for ductile fracture) and two-parameter (*J–Q* and *J–T*) characterizations. O'Dowd and Shih [3,4] and Sharma and Aravas [5] show the important role played by higher order terms in asymptotic solutions of crack-tip fields and demonstrate that a two-parameter characterization of the crack-tip fields involving *J* and a triaxiality or constraint parameter *Q* is necessary to satisfactorily describe the configuration dependence of fracture response of isotropic plastic solids, particularly under large scale yielding conditions. Rice [6] also notes the strong configuration dependence of the near-tip deformation fields, and that his asymptotic solution may not

* Corresponding author. Tel.: +1 352 392 0856; fax: +1 352 392 1071.
E-mail addresses: shawn350@ufl.edu (S.A. English), nagaraj@ufl.edu (N.K. Arakere), phillip.a.allen@nasa.gov (P.A. Allen).

0013-7944/$ - see front matter © 2009 Elsevier Ltd. All rights reserved.
doi:10.1016/j.engfracmech.2009.09.012

Nomenclature

t	thickness of the metallic section
t_b	thickness of the bonded section
a	crack depth
c	half crack width
r	radial distance from crack tip
J	J-integral
T	T-stress
σ_o	reference stress (defined for Ramberg–Osgood material)
r^*	normalized radial distance from crack tip ($r^* = r/(J/\sigma_o)$)
τ	normalized T-Stress ($\tau = T/\sigma_o$)
σ_∞	nominal stress of metallic section in the crack opening direction
Σ_∞	normalized nominal stress of metallic section ($\Sigma_\infty = \sigma_\infty/\sigma_o$)
θ	angle in-plane perpendicular to crack front, $\theta = 0^\circ$ is in the growth direction of the crack plane
ϕ	angle measured along the crack front in the crack plane

be applicable under large scale yielding conditions to low constraint fracture geometries such as center crack tensile (CCT) or single edge notch tensile (SENT) specimens, where the stresses around the crack tip may be much lower.

The applicable limits of J–T two-parameter characterization of elastic–plastic crack-tip fields using modified boundary layer (MBL) solutions have been explored by many investigators [7–9] for through-crack specimens. Wang [8] extended the two-parameter characterization with MBL reference solutions to topographical planes perpendicular to the crack front in surface crack tension (SCT) and surface crack bend (SCB) geometries. In addition to verifying the applicability of MBL solutions for J–T limit determination in surface-cracked plates, this study quantitatively explains the short falls of plane strain characterization of this geometry. Shih et al. [10] and O'Dowd [11], in addressing the limitations of plane-strain references applied to three-dimensional geometries, suggested that as r becomes small, the out-of-plane (parallel to the crack front) strains become small when compared to in-plane strains. Therefore, plane-strain MBL prediction of crack-front stress fields should be accurate as r approaches zero. The general conclusion was that a completely consistent two-parameter description of crack-tip stress fields is not possible beyond certain loads but is effective in determining the deformation limits of such characterization.

The characterization of tip fields and fracture prediction of metal liners with surface cracks bonded to an elastically loaded structural backing has not been well established. The fracture prediction of such structures is of intrinsic and practical interest with wide application in bonded pressure vessel technology such as composite overwrapped pressure vessels (COPV). For example, NASA's next generation Ares launch vehicles and the Orion spacecraft will have mission critical metal lined COPVs. COPVs generally consist of a thin (0.76+ mm) metallic (typically aluminum, titanium or stainless steel) inner liner wrapped with a comparatively thick (greater than three times the liner thickness) composite shell, commonly made from carbon/epoxy. The shell/wrap serves as the primary structural component, with the liner supporting very little load, but acts as a barrier for leakage of propellants and other pressurants. Understanding the behavior of surface cracks in COPV liners is challenging because, (i) the liner may have experienced initial plastic deformation during manufacturing processes, (ii) liner may experience cyclic plastic strains during normal operation, and (iii) surface crack behavior may be strongly influenced by the constraint effects resulting from the bonding. From a fundamental fracture mechanics perspective, we would like to understand the constraint effects that arise from the thin liner bonded to a stiff composite and its role in characterizing crack-tip fields.

This study will investigate if a SCT geometry that is not well characterized by J and T at larger loads, will maintain J–T predicted stress fields for loads beyond yield when bonded to an elastic structure. This will assess the applicability of the J and T parameters for predicting fracture at loads seen in a typical COPV. Although the liner loading in a COPV is likely to be more complicated, assessing the effects of this uniaxial structure will aid in standardized specimen development that can be used to characterize this situation.

2. *J–T* characterization of crack-front stress fields in surface-cracked plates

For non-standard geometries, fracture predictions using standard test specimens are reliant upon the ability to predict the stress field within the damage zone around the crack tip. The limit of stress field prediction can be expressed as a region (annulus) around the crack tip or a load for a specific geometry and loading condition. Within this limit, stress fields can be compared directly, and damage prediction can be made from single (high constraint) and two-parameter (low-constraint) measurements.

Two-parameter characterization uses a measure of the asymptotic fields, such as the stress intensity factor K, crack-tip opening displacement (CTOD) or the J-integral with an additional constraint parameter, such as the T-stress or stress difference Q, to predict crack-front stress fields. "Dominance" refers to the state in which the fracture and constraint parameters accurately represent the near crack stress state for a given geometry and loading condition. For loads causing deformation

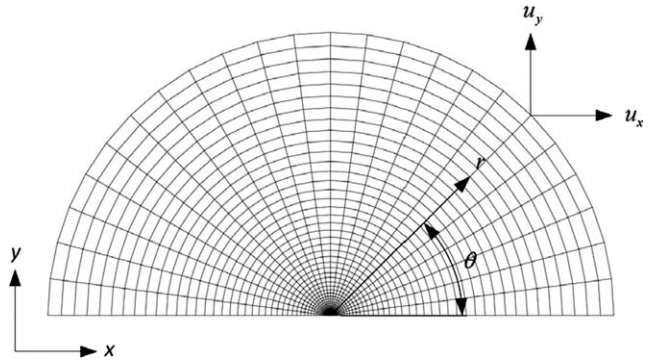

Fig. 1. MBL mesh and displacement boundary conditions.

beyond the dominance limit, the near crack stress fields are said to have plastically collapsed. Low crack tip constraint is characterized by negative *T*-stresses. Geometries with negative *T*-stresses do not maintain single parameter *J*-dominance. However, negative *T*-stress geometries can be described by *J*-integral and *T*-stress up to and exceeding net section yield [12]. *T*-stress is not defined under fully yielded conditions; nevertheless elastically scaled *T*-stresses calculated from far-field loads in elastic–plastic models are a relatively accurate constraint measurement for two-parameter characterization [8].

Determining two-parameter dominance relies on the ability to model idealized stress fields within the characterized range. This is done by use of modified boundary layer (MBL) solutions. The MBL solutions for this analysis are representative of the plane-strain elastic stress fields outside crack tip plastic zone under contained plasticity. Plane-strain approximation has proven to be valid in three-dimensional geometries as r approaches zero because the out-of-plane strain components will become small compared to the in-plane singular fields [10,11]. Therefore, near crack stress fields in surface cracked geometries should converge to the plane-strain MBL predicated reference fields.

The first two terms of the Williams eigen-expansion [13] approximate the stress state about the crack tip,

$$\sigma_{ij}(r,\theta) = \frac{K_I}{\sqrt{2\pi r}} f_{ij}(\theta) + T\delta_{1i}\delta_{1j} \tag{1}$$

where K_I is the mode I stress intensity factor and T is the T-stress. Fig. 1 shows the half-symmetric plane-strain FE mesh used for MBL analysis. The first two terms of the Williams series are applied as displacement boundary to the $r = r_{max}$ outer surface. The corresponding in-plane displacements are given by

$$u_i(r,\theta) = \frac{K_I}{E}\sqrt{\frac{r}{2\pi}} g_i(\theta,\nu) + \frac{T}{E} r h_i(\theta,\nu) \tag{2}$$

where E and ν are material constants and g_i and h_i are the angular variations in displacement caused by elastic singularity fields and T-stresses respectively [9]. Plane-strain MBL solutions for elastic–plastic crack-tip fields can be obtained by applying these displacements to the outer boundary of the circular crack tip region and varying the T-stress while K_I remains constant. The J-integral is related to the stress intensity factor K_I in plane strain by:

$$J = \frac{1-\nu^2}{E} K_I^2 \tag{3}$$

Abaqus version 6.7 [14] was used to compute the MBL solutions for a low strain hardening Ramberg–Osgood material with a range of negative T-stresses. Fig. 2 shows the near crack opening-stress fields predicted by our MBL model.

Wang [8] showed that these MBL solutions provided accurate prediction of stress fields in SCT specimens as characterized by J and T, and that the crack-tip fields of the MBL solution far from the outer boundary and outside the crack-tip blunting zone should represent those of any crack with the same K_I and T. Therefore, stress fields in topographical planes perpendicular to the crack front of the SCT geometry that accurately compare to the MBL reference solutions are said to have J–T dominance.

3. Finite element models

3.1. Material description

The Ramberg–Osgood power law hardening material model intrinsic to the deformation plasticity theory with Abaqus was used for this analysis. This model is defined by the following equation,

$$\frac{\varepsilon}{\varepsilon_o} = \frac{\sigma}{\sigma_o} + \alpha\left(\frac{\sigma}{\sigma_o}\right)^n \tag{4}$$

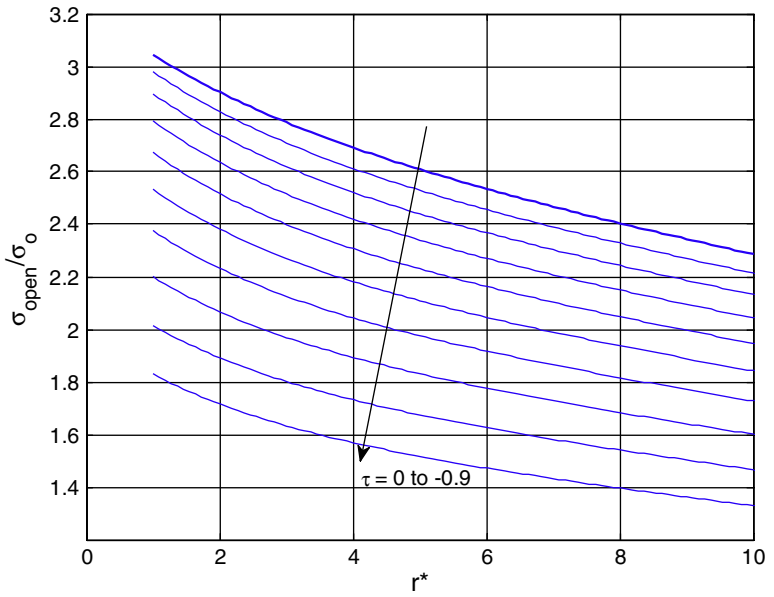

Fig. 2. Plane-strain MBL normalized near crack opening stresses for negative T-stresses. The thick line corresponds to zero τ (SSY solution) where $\tau = T/\sigma_o$ *and* $r^* = r\sigma_o/J$.

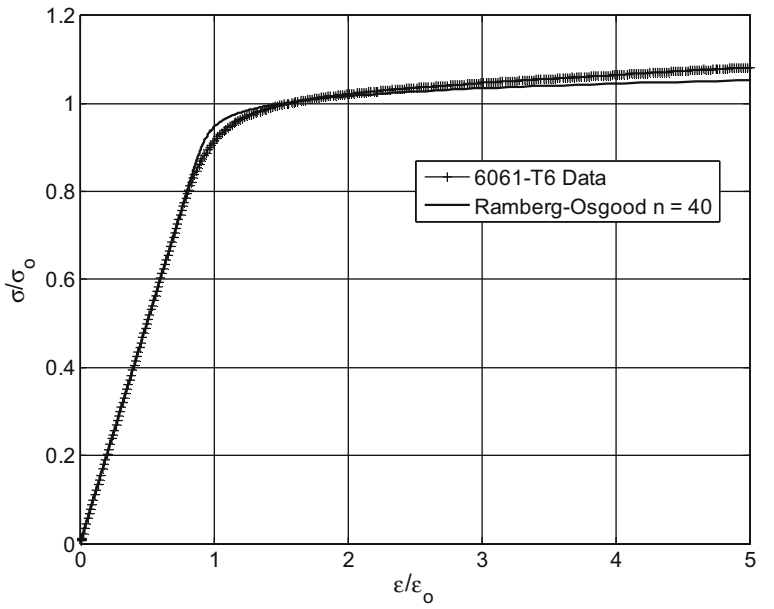

Fig. 3. Ramberg–Osgood material models for a low ($n = 40$) strain hardening material and 6061-T6 aluminum test data from a $t = 1.27$ mm (0.05 in.) thick plate under uniaxial tension.

$$\varepsilon_o = \frac{\sigma_o}{E} \tag{5}$$

where E is the Young's modulus, σ_o is the reference yield strength, n is the strain-hardening exponent, and α is the fitting coefficient or strain offset. A low strain hardening material, with a true stress–strain curve seen in Fig. 3, was used for our analysis with the following parameters: $E/\sigma_o = 250$, $\alpha = 0.5$, $n = 40$ and the Poisson ratio $\nu = 0.33$. When using the Ramberg–Osgood material model, a low strain hardening material will minimize the nonlinear effects of scaling T-stresses with fully elastic models. This material model was studied because of its simplicity and similarities to the 6061-T6 aluminum currently being tested for use in NASA's future COPVs. The uniaxial tensile data for a $t = 1.27$ mm (0.05 in.) thick plate specimen is also given in Fig. 3 to demonstrate the similarities.

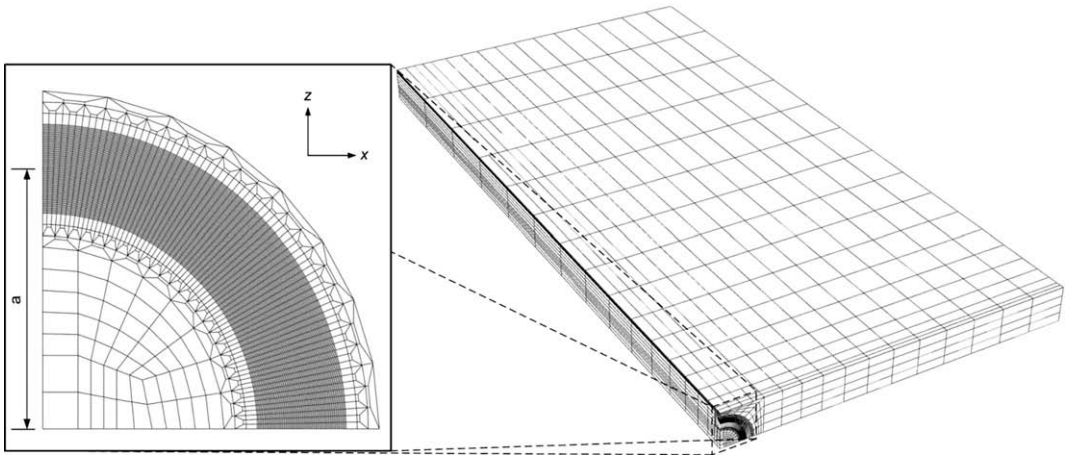

Fig. 4. FEA visualization of the surface crack face and contour region.

Table 1
Dimensions of models used in the analysis (a = 0.889 mm (0.035 in.)).

Model	Type	t_{Liner} (mm)	$t_{Backing}$ (mm)	t_{Total} (mm)	a/t_{Liner}	a/t_{Total}
1	Bonded	1.27	3.81	5.08	0.7	0.175
2	Homogeneous	1.27	N/A	1.27	0.7	0.7
3	Homogeneous	1.778	N/A	1.778	0.5	0.5
4	Homogeneous	2.54	N/A	2.54	0.35	0.35
5	Homogeneous	5.08	N/A	5.08	0.175	0.175

COPVs consist of a thick, relative to the liner, composite shell. This shell consists of multiple overlapping carbon fiber epoxy layers wound at different angles relative to the vessels axis comprising the layup. For the uniaxial tension specimen of interest, the strain distributions and constraint in the thickness direction will be significantly different from the complex loading seen in a COPV. Thus, the anisotropic material effects would be difficult to isolate and significantly complicate the analysis. Therefore, an isotropic linear elastic material with uniaxial stiffnesses ranging from three times the liner modulus, typical of a carbon epoxy in the fiber direction, to equal to the liner modulus ($E_{Backing}/E_{Liner}$ = 1, 2, 3) with a Poisson's ratio of ν = 0.33 was used. This model will assess the effects of maintaining partial elasticity within the layered geometry while the cracked portion undergoes large-scale plastic deformation.

3.2. Geometry and FE mesh

FEA Crack version 3.1.14 [15] was used to generate the crack mesh and Abaqus version 6.7 [14] was used for the analysis. Both an elastic–plastic model and a fully elastic model for each of the geometries tested are necessary. The elastic–plastic model is used to calculated opening-stress fields and J-integrals. The fully elastic model is used to find the T-stress scaling factors ($T(\phi)$), which are normalized by the nominal stress in the opening direction (σ_∞) of the metallic section. The J-integrals along the crack front are calculated using the domain integral method applied to three dimensions intrinsic to Abaqus. The T-stresses are calculated using the interaction integral method intrinsic to Abaqus in the fully elastic models [16].

The finite element analyses are made using C3D20R 20-node isoparametric brick elements. At the crack-tip, 20-node collapsed face prismatic elements are used. To allow for crack-tip blunting in the elastic–plastic models, the initially coincident nodes at the crack tip are left unconstrained. In order to maintain sufficient data points at the desired r^* values, the crack region contains a highly refined mesh consisting of 31 contours around the crack tip and 72 collapsed face elements along the crack front. Fig. 4 shows the crack face mesh with these refinements. A study of mesh refinement was conducted by comparing T-stress measurements, which tend to be sensitive to mesh refinement, from various models of mesh density. With increasing mesh refinement, the T-stresses converged to stable values and continued through the mesh refinement used for this analysis. The chosen mesh refinement is beyond the level needed for accurate stress and interaction integral calculations, but was necessary to achieve sufficient radial data points to assess the opening stress field.

The FE cracked plate implemented in the bonded geometry contains a semicircular surface crack with a depth of a = 0.889 mm (0.035 in.) central in a $w \times l \times t$ = 25.4 × 50.8 × 1.27 mm (1 × 2 × 0.05 in.) plate. The thickness of the backing is chosen to be three times the cracked plate thickness ($t_b \approx 3t$) which is a good approximation for a COPV overwrap. In order to compare the relative accuracy of crack tip characterizations between the bonded model and unbonded models (SCT), various thicknesses t = 1.27, 1.78, 2.54, 5.08 mm (t = 0.05, 0.07, 0.10, 0.20 in.) are implemented for the homogeneous surface cracked models with a constant crack size a = 0.889 mm (0.035 in.), shown in Table 1.

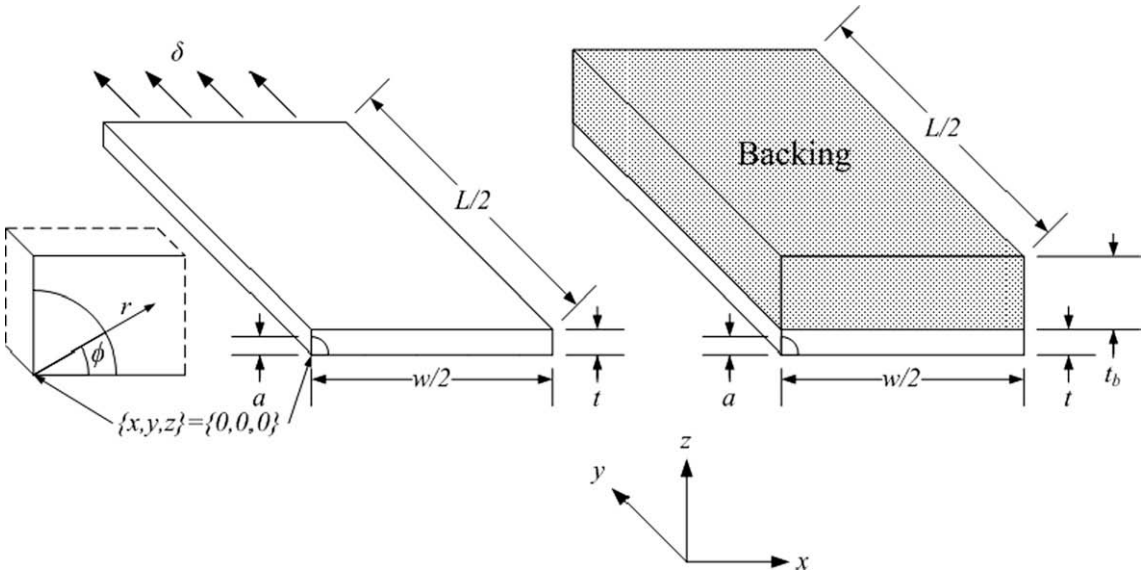

Fig. 5. Schematic of the quarter symmetry SCT specimen model.

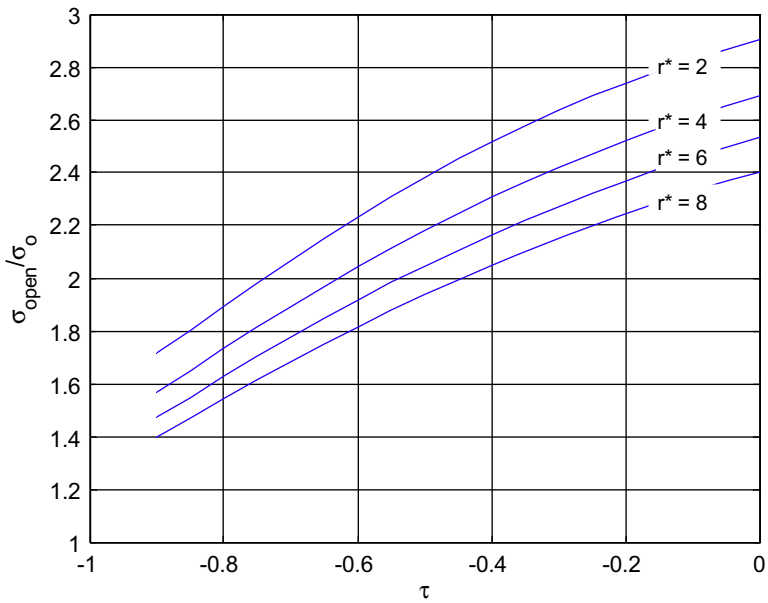

Fig. 6. MBL opening stress references as a function of $\tau = T/\sigma_o$ for the material with strain hardening coefficient $n = 40$.

The FE model contains two planes of symmetry, thus the model shown in Fig. 5 constitutes one quarter of the complete coupon. A zero displacement boundary condition ($u_i(x, y, z) = 0$) was applied to the node at (0, 0, t_{Total}) to eliminate rigid body motion, where $t_{Total} = t_{Liner} + t_{Backing}$. The bonded model used Abaqus tie constraints to "adhere" the metallic plate to the composite backing. A tie constraint couples the nodal displacements of the slave surface, in this case the metallic section, to the surface displacement field of the master surface (composite section).

Crack-tip blunting effects can typically be neglected at distances roughly twice the crack-tip opening displacement or $2J(\phi)/\sigma_o$. Inside this distance from the crack tip, it would be necessary to use large strain analysis [12]. For this investigation, small strain approximation will be used to analyze stress fields outside the crack-tip blunting zone.

3.3. Data reduction

The nodal opening stresses (σ_{yy}) were obtained from the contour region perpendicular to the crack front. Software was produced to obtain these values and the corresponding radial distances (r) at various crack-front angles (ϕ). Radial distance

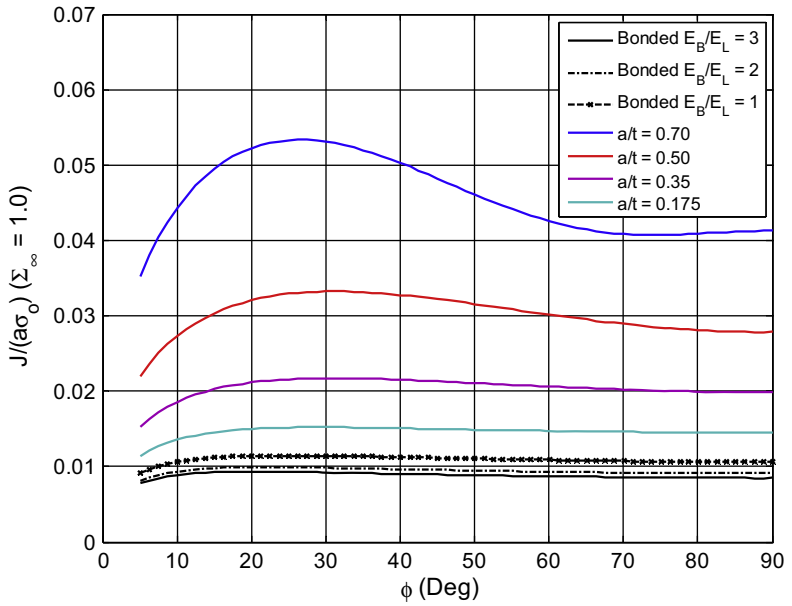

Fig. 7. *J*-integral as a function angle ϕ at a constant nominal load $\Sigma_\infty = 1.0$.

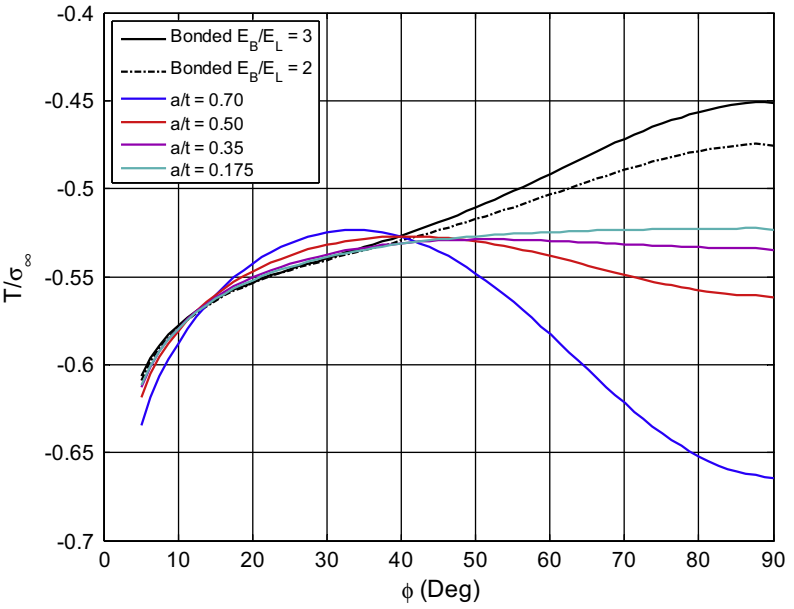

Fig. 8. *T*-stress scaling factor as a function of angle ϕ.

was measured perpendicular to the crack front in the $\theta = 0^\circ$ plane of the un-deformed configuration. *J*-integrals were calculated at each circular contour. The mean *J*-integrals at each crack angle ($J(\phi)$) were calculated by averaging the values from contours 20 through 30, in which the *J*-integral varied by a negligible amount (<0.10%). Similarly, the *T*-stress values were obtained from the elastic models and used to calculate an elastic *T*-stress scaling factor ($T(\phi)/\sigma_\infty$). This factor assumes a constant linear relationship between *T*-stress and nominal stress. For the elastic–plastic models, the nominal stress in the opening direction σ_∞ was used to estimate the *T*-stresses. The nominal stresses were calculated from the center of an un-cracked geometry.

Opening stresses in the crack plane ($\theta = 0^\circ$) are plotted as functions of normalized radial distance $r^* = r\sigma_o/J(\phi)$ from the crack tip, then the stresses are interpolated at constant r^*-values, where σ_o is the reference yield strength defined in the Ramberg–Osgood material model and $J(\phi)/\sigma_o$ is an approximation of the blunting zone size or crack-tip opening displacement.

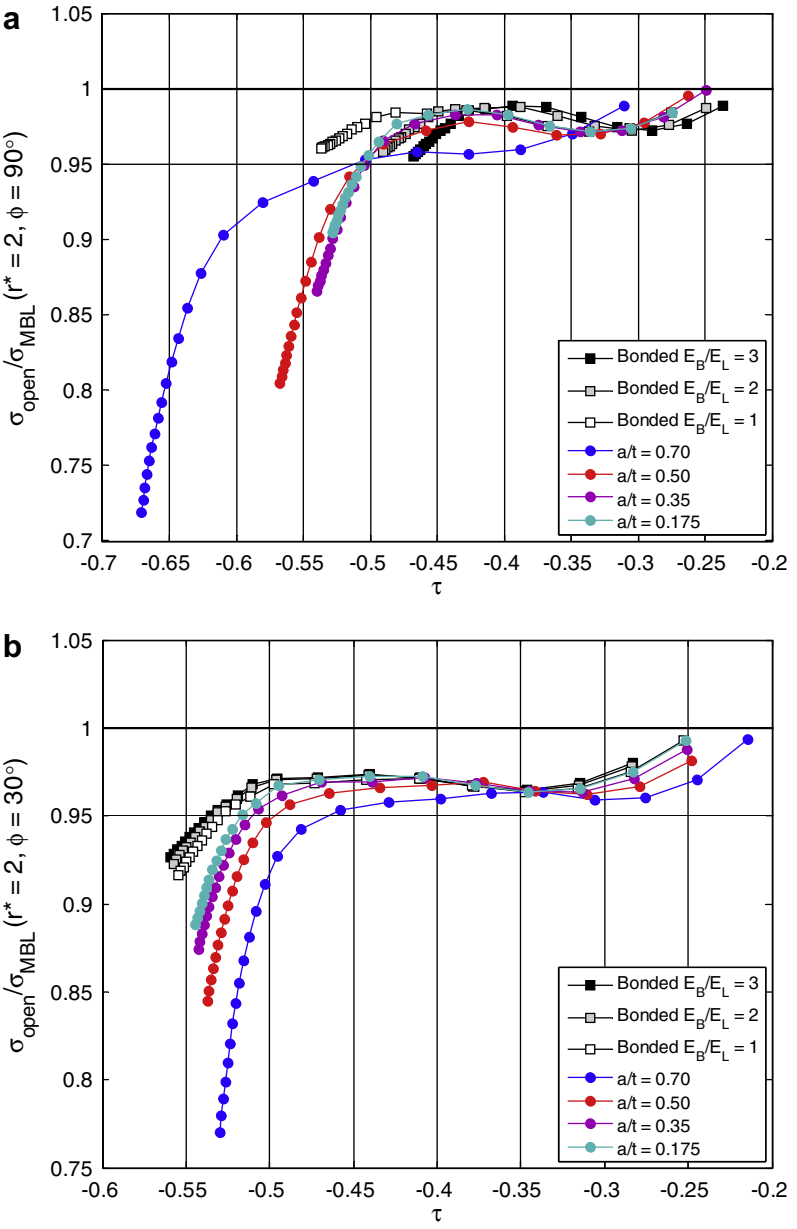

Fig. 9. Opening stress normalized by MBL reference solutions as a function of normalized T-stress τ at $r^* = 2$ and (a) $\phi = 90°$ and (b) $\phi = 30°$.

Similarly, MBL data is analyzed at constant r^*-values producing the J–T characterized opening stress references as a function of constraint value T, Fig. 6. The data presented in this analysis is normalized by these MBL reference solutions. In addition to constraint comparison, the data is also presented as a function of load level (σ_∞).

4. Results and discussion

4.1. J-integral and T-stresses

Fig. 7 show the J-integral calculations at constant load of $\sigma_\infty = \sigma_o$ or $\Sigma_\infty = 1.0$. The decreasing trend due to the thickness effects on the crack opening is typical of J-integral calculations. The bonded cases shows significant reduction in J when compared to the case of equal total thickness ($a/t = 0.175$). This discrepancy is simply due to the differences in strain distribution on the plane of the bond and the equivalent plane in the homogeneous models caused by the continued partial elasticity of the structure. The bonded structures will have a more uniformly distributed strain field on this plane resulting in lower

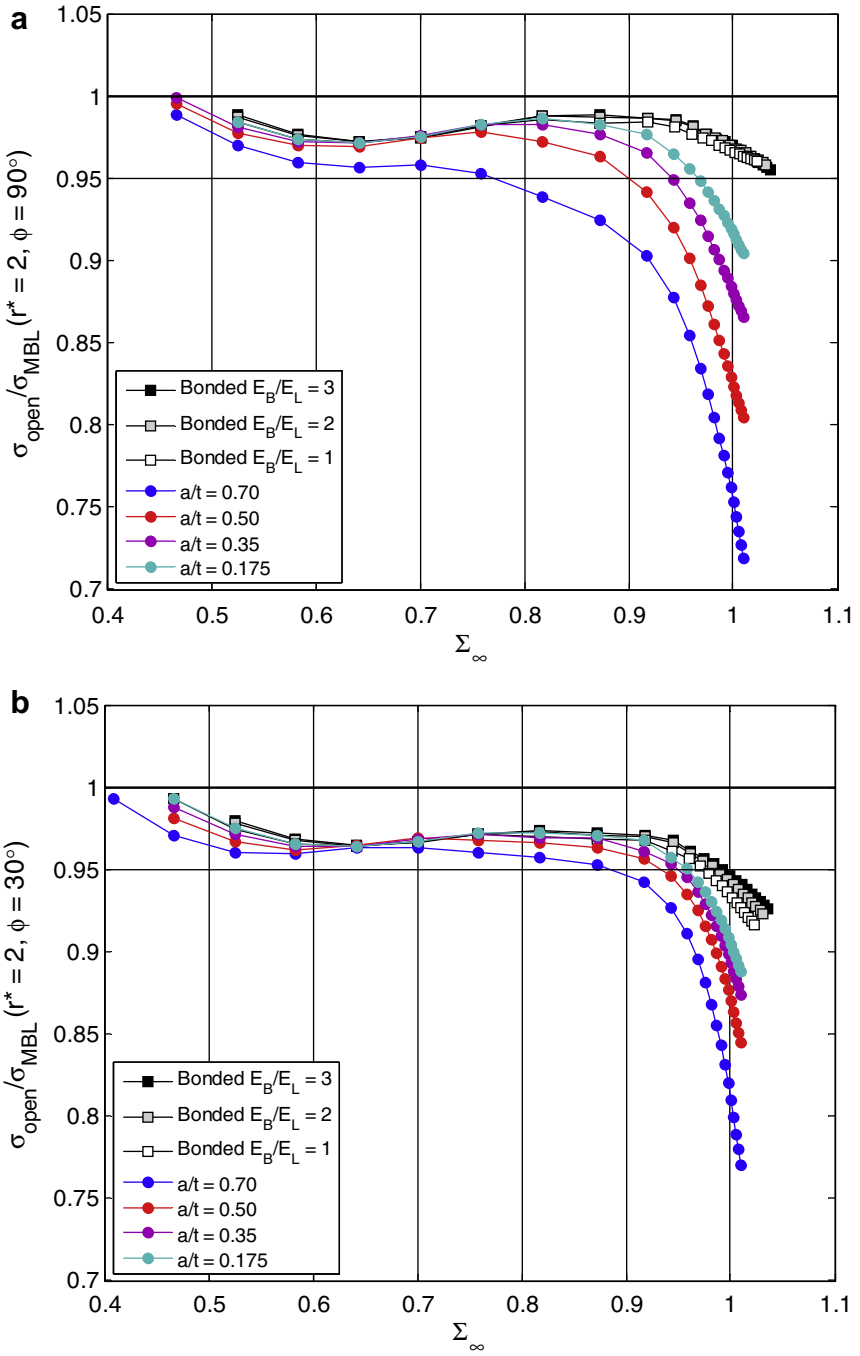

Fig. 10. Opening stresses normalized by MBL reference solutions as a function of normalized nominal stress Σ_∞ at $r^* = 2$ and (a) $\phi = 90°$ and (b) $\phi = 30°$.

opening displacements near the crack for a given load. By comparing the bonded model with $E_{Backing}/E_{Liner} = 1$ to the homogeneous model of equivalent total thickness ($a/t = 0.175$), which under elastic loading are identical, it is shown that the effects of continued partial elasticity on this structure is the primary cause for lowered J values at loads causing sufficient plastic deformation. Similarly, the effects of modulus ratio in the bonded models on the J-integral, although not significant at these loads, can explain the decrease in J with the increase in modulus. Observing that the J values from the bonded case are closer in magnitude to those of the equivalent thickness model ($a/t = 0.175$), supports the claim that the effective thickness of the liner increases when bonded to an elastic structure from a fracture standpoint. In fact, this effective thickness is most likely greater than the total composite/liner model thickness. This postulate is supported further when looking at J–T dominance of opening-stress fields.

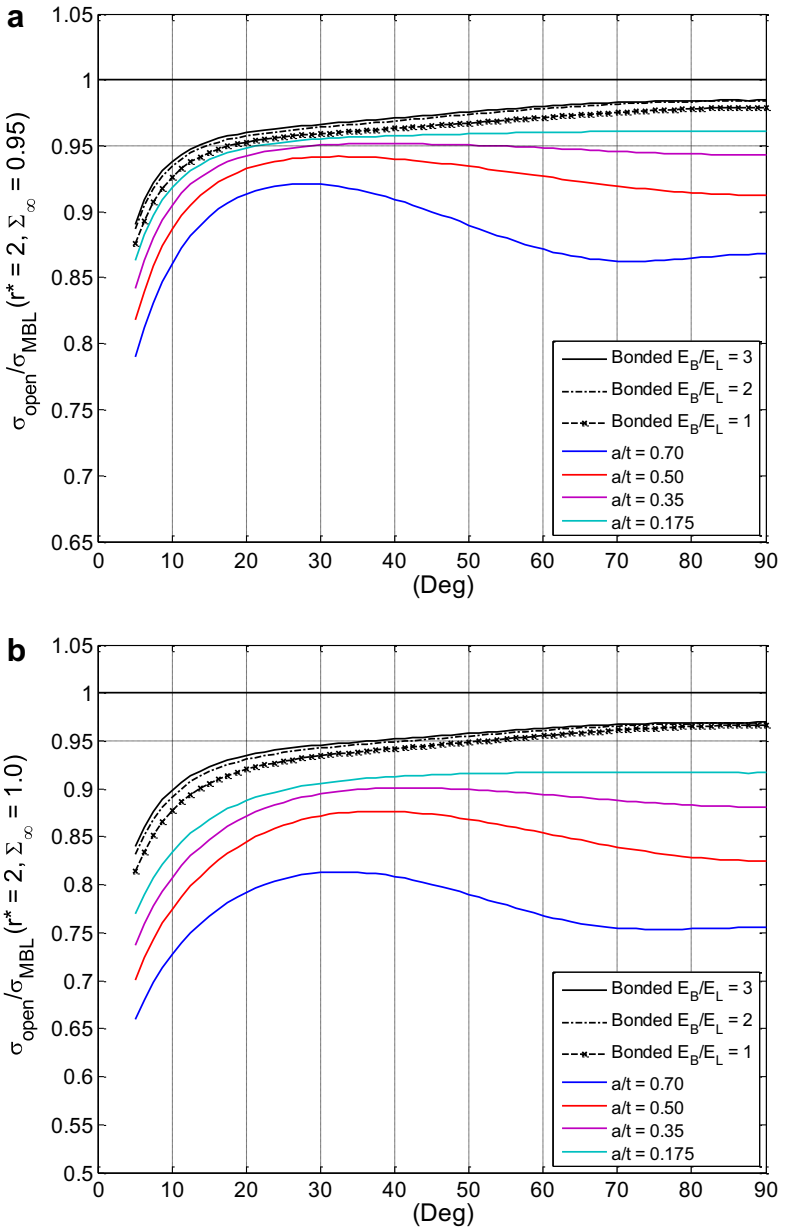

Fig. 11. Opening stresses normalized by MBL reference solutions as a function of angle ϕ at $r^* = 2$ and (a) $\Sigma_\infty = 0.95$ and (b) $\Sigma_\infty = 1.0$.

Fig. 8 gives the T-stress scaling factors (T/σ_∞) at various angles ϕ calculated from each of the models with linear elastic material properties. The homogeneous models show a trend typical of T-stresses for increasing thickness. The bonded models however show a much stronger trend and are highly dependent upon modulus ratio. When the modulus ratio is unity, the elastic geometry is equivalent to the $a/t = 0.175$ homogeneous case. The T-stresses near the bonded surface ($\phi > 40°$) for the bonded models with modulus ratios of 2 and 3 are higher when compared to the homogeneous models. Conversely, for angles near the free surface ($\phi < 40°$) the discrepancies seem insignificant. These trends of course become heavily dependent on material properties like the ratio of moduli and anisotropy and are not clearly representative of the extent of two-parameter dominance before plastic collapse.

4.2. Opening-stress fields

The most obvious and significant comparison with regard to the fracture driving force is of the opening stresses in the crack plane ($\theta = 0°$) as functions both a constraint parameter (T-Stress) and the applied load level (σ_∞). The opening stress

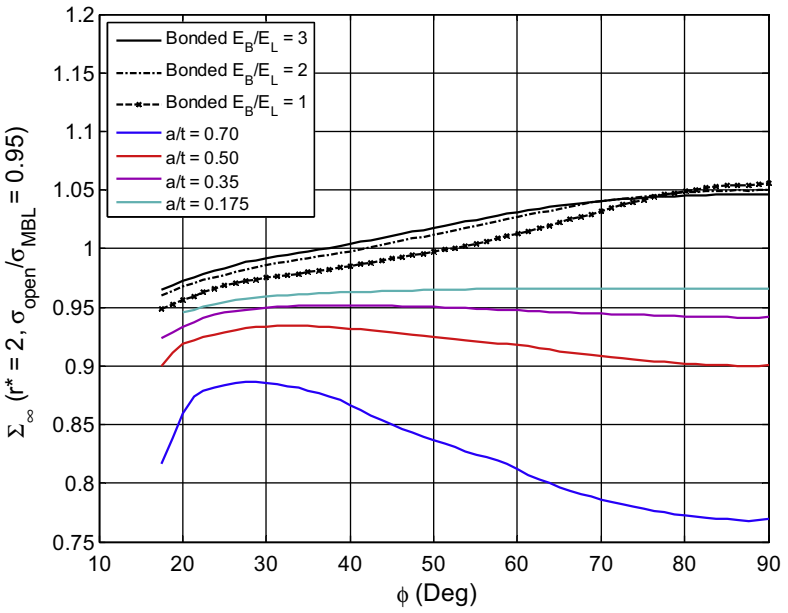

Fig. 12. Normalized nominal load Σ_∞ at opening stresses corresponding to plastic collapse ($\sigma_{open}/\sigma_{MBL} = 0.95$) at various crack angles ϕ.

normalized by the plane-strain MBL reference solutions at *T*-stresses corresponding to those scaled by the nominal load in the surface cracked model and $r^* = 2$ are given as a function of normalized *T*-stress τ for angles $\phi = 90°$ and 30° in Fig. 9a and b, respectively. These curves show the effect of increasing *T*-stress and consequently increasing nominal load on two-parameter opening stress characterization. Due to the varying *T*-stress scaling factors and the fact that *T*-stress alone is not sufficient to determine two-parameter dominance; it is more beneficial to look at opening stresses as a function of nominal load on the metallic section.

Fig. 10a and b give the opening stress normalized by the plane-strain MBL reference solutions and $r^* = 2$ as a function of nominal load on the metallic surface for angles $\phi = 90°$ and 30°, respectively. The bonded cases show a greater adherence to the MBL predicted opening stresses for higher load levels when compared to those of the homogeneous models. Increasing thickness corresponds to an increase in load level in which *J*–*T* dominance is sustained. The modulus ratios in the bonded models do not have a significant effect on the dominance limit load. When the modulus ratio is unity in the bonded model and $a/t = 0.175$ for the homogeneous model, Figs. 9 and 10 a and b shown that the results are identical under low loads, but diverge as deformation increases.

Normalized opening stresses are shown as a function of crack angle ϕ at constant normalized far-field loads $\Sigma_\infty = 0.95$ and 1.0 in Fig. 11a and b, respectively. These curves give insight into how two-parameter dominance varies with crack angle. It becomes necessary when ϕ becomes small (near the free surface) to ignore angles $\phi < 5°$ because HRR singularity will only be present at near crack points embedded entirely in material [17]. Therefore, Fig. 11a and b show opening stresses for angles $\phi > 5°$. The following observations are made when comparing the bonded cases to the four homogeneous models. At both the loads examined, the bonded cases show greater adherence to *J*–*T* characterized fields. At a nominal load of $\Sigma_\infty = 0.95$ only the bonded cases and the thickest homogeneous case ($a/t = 0.175$) have not yet shown signs of plastic collapse for angles $\phi > 21°$. At a load equaled to far-field yield ($\Sigma_\infty = 1.0$) all the homogeneous models have lost *J*–*T* dominance, which is arbitrarily characterized be deviation from the MBL solution by 5%. For both loads, when the thickness of the homogeneous specimen is doubled ($a/t = 0.35$ to $a/t = 0.175$) the opening stresses are only slightly closer to those predicted by the MBL solutions. This is in contrast to the significant difference that can be seen in the transitions between $a/t = 0.70$, 0.50 and 0.35. The asymptotic function of thickness is well established as *t* approaches infinity and is important when comparing results to a non-homogeneous structure and the implications of an "equivalent thickness" homogeneous specimen.

Fig. 12 gives the nominal stresses in the opening direction at which the opening stresses at a constant normalized radial distance $r^* = 2$ deviate from the predicted plane-strain MBL stresses by 5%. This point is arbitrarily called the point of field collapse, in which *J* and *T* no longer characterize the stress state within tolerable limits due to excessive plastic deformation. The bonded geometries exhibit higher *J*–*T* dominance for loads exceeding far field yielding when compared to the other homogeneous models. The homogeneous surface cracked models are approaching a limiting thickness in which further increase will not add to the limit load for *J*–*T* characterization. This is most clearly seen in $a/t = 0.35$ and $a/t = 0.175$. Though the thickness is doubled, there is only a small change in limit load between these two geometries. This limitation of thickness effects may prevent the design of an "equivalent thickness" homogeneous structure that would have the same fracture characteristics as the bonded model, but will provide quantifiable limits to using homogeneous structures to represent bonded configurations.

5. Conclusions

The goal of this study is to determine the feasibility of using *J* and *T* fracture parameters in characterizing crack-tip stress fields in a surface cracked liner bonded to an elastic structure for loads typical to a COPV. The loads seen in a COPV liner exceed the yield strength in both manufacturing and normal operation; therefore, fracture characterization at these loads is critical. The bonded curves in Fig. 12 show that a simple two-parameter model for opening stresses in a metallic composite uniaxial structure can be used for loads seen in COPVs. From this analysis, it can be concluded that *J*–*T* characterization may be applicable for uniaxial tension of bi-material bonded specimens and pressure loadings of COPV test specimens at these high loads, but simple homogeneous uniaxial tension specimens do not provide a fracture equivalent geometry that maintains the level of *J*–*T* dominance seen in the composite geometries. The difference of continued *J*–*T* characterization in homogeneous models at large loads stems from the inability to maintain the elastic constraint effects of the backing. For bi-material uniaxial test specimens, the effect of the backing to liner modulus ratio does not appear to be great within the tested range indicating the most significant influence of the backing is its ability to impose an elastic constraint on the liner even at very high levels of far field loading.

Acknowledgements

The authors express their appreciation for the support provided by the NASA Marshall Space Flight Center (MSFC). Ongoing, unpublished research at MSFC concerning the deformation limits for surface crack testing laid the foundation for many of the analytical tools and techniques used in this study. The authors also thank the NASA Langley Research Center (LARC) for providing us with specimen data.

References

[1] Leach AM, Daniewicz SR, Newman Jr JC. A new constraint based fracture criterion for surface cracks. Engng Fract Mech 2007;74:1233–42.
[2] Evans AG, Riley PL. Progress in nitrogen ceramics. The Netherlands: Martinus Nijhoffm Publisher; 1983. p. 595.
[3] O'Dowd NP, Shih CF. Family of crack-tip characterized by a triaxiality parameter—I. Structure of fields. J Mech Phys Solid 1991;39:989–1015.
[4] O'Dowd NP, Shih CF. Family of crack-tip characterized by a triaxiality parameter—II. Fracture applications. J Mech Phys Solid 1992;40:936–9.
[5] Sharma SM, Aravas N. Determination of higher-order terms in asymptotic elastoplastic crack tip solutions. J Mech Phys Solid 1991;39:1043–72.
[6] Rice JR, Rosengren GF. Plane strain deformation near a crack tip in a power-law hardening material. J Mech Phys Solid 1968;16:1–12.
[7] Newman Jr JC, Bigelow CA, Shivakumar KN. Three-dimensional elastic–plastic finite-element analyses of constraint variations in cracked bodies. Engng Fract Mech 1993;46:1–13.
[8] Wang YY. On the two-parameter characterization of elastic–plastic crack-front fields in surface-cracked plates. In: Hackett EM, Schwalbe KH, Dodds RH, editors. Constraint effects in fracture ASTM STP 1171. Philadelphia, PA: American Society for Testing and Materials; 1993. p. 120–38.
[9] Wang YY, Parks DM. Limits of *J*–*T* characterization of elastic–plastic crack-tip fields. In: Kirk M, Bakker A, editors. Constraint effects in fracture theory and applications: second volume ASTM STP 1244. Philadelphia, PA: American Society for Testing and Materials; 1995. p. 43–67.
[10] Shih CF, O'Dowd NP, Kirk MT. A framework for quantifying crack tip constraint. In: Hackett EM, Schwalbe KH, Dodds RH, editors. Constraint effects in fracture ASTM STP 1171. Philadelphia, PA: American Society for Testing and Materials; 1993. p. 2–20.
[11] O'Dowd NP. Applications of two parameter approaches in elastic–plastic fracture mechanics. Engng Fract Mech 1995;52:445–65.
[12] Betegón C, Hancock JW. Two-parameter characterization of elastic–plastic crack-tip fields. J Appl Mech 1991;58:104–10.
[13] Williams ML. On the stress distribution at the base of a stationary crack. J Appl Mech 1957;24:111–4.
[14] Dassault Systèmes. ABAQUS Version 6.7-4. Providence, RI: Dassault Systèmes; 2007.
[15] Quest Reliability LLC. FEA-Crack Version 3.1.14. Boulder, CO: Quest Reliability LLC; 2007.
[16] Dassault Systèmes. ABAQUS theory manual. Providence, RI: Dassault Systèmes; 2007.
[17] Wang X. Two-parameter characterization of elastic–plastic crack front fields: surface cracked plates under tensile loading. Engng Fract Mech 2009;76:958–82.